Author

Jean-Marie Fleureau is associate professor of soil mechanics and hydraulics at the Ecole Centrale de Paris. He heads a research group of eight people whose main aim is the study of the mechanical, hydric, and interfacial properties of polyphasic granular materials. Fleureau holds a BE degree in civil engineering and a PhD degree in mechanics from the Ecole Centrale de Paris.

35. Blake, T.D. and Haynes, J.M.: "Contact Angle Hystersis," *Progress in Surface & Membrane Sci.*, J.F. Danielli, M.D. Rosenberg, D.A. Cadenhead (eds.), (1973) **6**, 125–38.
36. Bayramli, E., Van De Ven, T.G.M. and Mason, S.G.: "Tensiometric Studies on Wetting, I. Some Effects of Surface Roughness," *Cdn. J. of Chemistry* (1981) **59**, No. 13, 1954–61.
37. Neogi, P. and Miller, C.A.: "Spreading Kinetics of a Drop on a Rough Solid Surface," *J. Colloid Interface Sci.* (April 1983) **92**, No. 2, 338–49.

SI Metric Conversion Factors

cp	× 1.0*	E−03	= Pa·s
°F	(°F−32)/1.8		= °C
in.	× 2.54*	E+00	= cm
lbm/gal	× 1.198 264	E−01	= g/cm³
md	× 9.869 233	E−04	= μm²

*Conversion factor is exact.

SPEFE

Original SPE manuscript received for review Oct. 9, 1989. Revised manuscript received June 20, 1991. Paper accepted for publication Jan. 24, 1992. Paper (SPE 19681) first presented at the 1989 SPE Annual Technical Conference and Exhibition held in San Antonio, Oct. 8–11.

Acoustic-Emission Monitoring During Hydraulic Fracturing

Lisa Stewart, Schlumberger-Doll Research; **B.R. Cassell,** SPE, Schlumberger Wireline Services; and **G.M. Bol,*** SPE, Nederlanse Aardolie Mij. B.V.

Summary. Microseismic events or acoustic emissions associated with hydraulic fracturing are recorded with a borehole seismic tool in a deviated well during multirate injection, shut-in, and flowback. The event locations indicate that fracture orientation, length, and height are compatible with regional stress directions and estimates of the fracture size that are based on pressure decline.

Introduction

Fractures, either natural or induced, can be the most important feature controlling the productivity of a hydrocarbon reservoir. Knowledge of their orientation, length, and height can affect all stages of planning and is especially important for horizontal drilling, stimulation of low-permeability reservoirs, in-fill drilling, and EOR programs.

Many methods have been developed to model or measure the characteristics of hydraulically induced fractures.[1] These include in-situ or regional stress studies, inference of material-strength properties from wireline logs, pressure-decline analysis, laboratory experiments on cores, and comparison of such pre- and postfracture logs as temperature, borehole images, gamma ray, and sonic. Most of these techniques investigate the fracture in the near-wellbore region and are successful only in open holes contained in the fracture plane.

The acoustic-emission-mapping technique was developed for applications in fracturing crystalline rock and has a history of success in such hot-dry-rock geothermal fields as Fenton Hill,[2,3] Camborne,[4] and Kakkonda.[5] Acoustic emissions have been used with varying degrees of success to map hydraulic fractures in sedimentary formations.[6-9] The high attenuation of seismic waves in sedimentary rocks imposes limitations in the instrumentation and acquisition configurations that can "listen" to fractures. Acoustic emissions may be thought of as microearthquakes, or microseismic events caused by brittle fracture in a region surrounding a hydraulic fracture. They are believed to be caused by a combination of stress release in the zone of high pore pressure surrounding the fracture and the presence of inhomogeneities in the formation. Laboratory experiments show that these events arise from discrete ruptures on the fracture plane.[10] If these microseismic events can be located, the strike and dip of the fracture can be determined. This provides a characterization of the fracture far from the borehole that can be implemented in cased or nonvertical wells, even for nonvertical fractures.

As in earthquake location, acoustic-emission location is more accurate when multiple receivers are used. The ideal situation is to deploy several vertical arrays of three-component sensors near the expected fracture to get accurate locations of many events by triangulation. Unfortunately, few hydrocarbon-reservoir sites present this opportunity. In principle, however, locations can be determined with a single calibrated three-component sensor, either in the injection well itself or in a nearby observation well. Assuming that the first motion created by the source mechanism is radially compressional (or dilatational), the polarization angle of the event's first-arrival compressional (P) wave defines the direction from receiver to event. This is a simple problem to solve in a homogeneous medium but is slightly more difficult in a layered medium because the seismic rays bend at interfaces. The difference in travel times between the P wave and the secondary, or shear (S) wave is related to the distance to the event. This location method requires knowledge of the P- and S-wave velocity structure near the fracture and careful placement of the sensor to ensure that all events occur above or below it. The latter requirement arises because the source mechanism is unknown: i.e., a P wave coming from above has the same signature as a dilatational wave from below. The first requirement, knowledge of the velocities, is often satisfied only in an approximate fashion: average velocities from prestimulation sonic logging, check shots, or vertical seismic profiles (VSP's) can give reasonable estimates, and poststimulation velocities may be slightly different. Green and Baria[11] reported a decrease of < 1% in P-wave velocities after injection treatment in crystalline rock.

Deriving the polarization information from seismic records requires tool calibration because the polarization calculation depends on the relative amplitudes recorded on the three axes. Calibration can be done *in situ* by clamping the tool at the level where the fracture recording will occur and locating a known energy source, such as an airgun shot, a buried charge, or a downhole source, in a nearby well.

Fracture-Mapping Survey

Objective. The objective of the experiment was to test the feasibility of an EOR program that would entail water injection above fracturing pressure if we could confirm that the fracture would not grow toward the producing well. By monitoring the seismic activity generated by high rate injection, the fracture orientation and propagation length can be determined.

Data Acquisition. The downhole equipment consisted of a modified slimhole seismic tool with a 2.125-in. OD and a 20,000-psi pressure rating. The locking device was a hydraulic arm. The modification involved replacing the triaxial geophone assembly with accelerometers so that we could record signals in the range of thousands of cycles/sec. The laboratory-calibrated accelerometers had a sensitivity of $1{,}000\times10^{-12}$ coulomb per unit gravitational acceleration with a linear response of more than 2,000 cycles/sec over a temperature range up to 482°F. These sensors were arranged orthogonally with the z axis tangential to the tool axis and the x axis in the same plane as the clamping arm, effectively the radial component. The relative bearing of the tool is given by the angle between the x axis and the vertical plane along the deviated borehole. This angle was measured by a circular potmeter attached to the tool housing. The wiper of the potmeter always points vertically because of an attached weight. During the survey, the x axis was at an angle of 27° to the vertical (**Fig. 1**, insert). Surface airgun sources were deployed to obtain an independent measurement of the tool orientation, effectively calibrating the relative response of the tool's three axes at the frequencies contained in the airgun signature. The surface shots, however, were not detected by the downhole accelerometers, probably because of the low-frequency content of the signals propagating from the source through soft sedimentary material. Because the surrounding area had a heavy surface buildup, it was not feasible to attempt other dangerous or destructive calibration techniques so we base our calibration on the laboratory accelerometer response.

Surface equipment was supplied by a subcontractor and consisted of amplifiers, a videocassette recorder, and a power supply for the downhole tool. Data were recorded in analog form on four 240-minute videocassette tapes, and the downhole signals were monitored on an oscilloscope during the survey.

Surface Configuration. The tool was run through 2.875-in.-ID tubing and clamped in 7-in. casing at a measured depth of 6,282.8 ft

*Now at Koninklijke/Shell E&P Laboratorium.

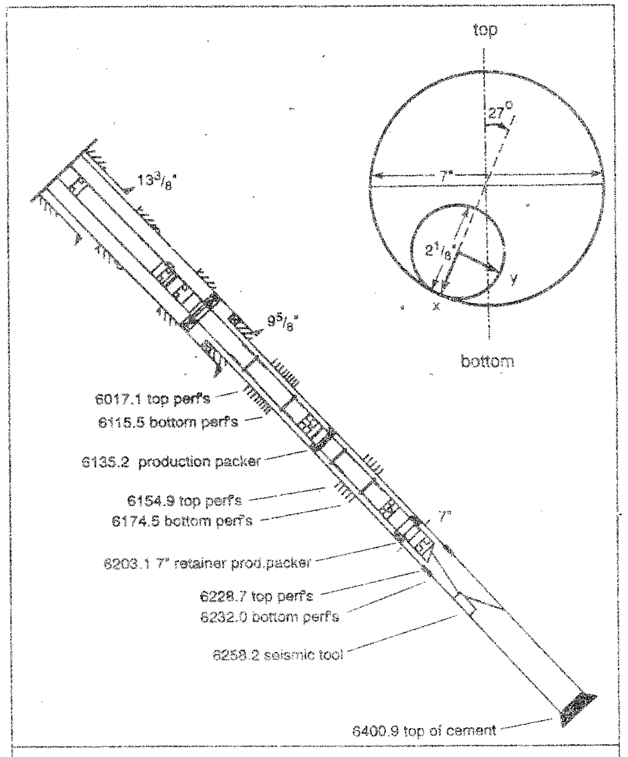

Fig. 1—Completion diagram. Recording tool was clamped below bottom of tubing, 24.6 ft below bottom perforations. Borehole deviation is 43° from vertical. Insert shows position of downhole recording tool looking down borehole. After coupling, the (radial) x axis was oriented 27° from the vertical plane containing the borehole.

from rotary table (RT), which is 26.2 ft above bottom flange, or 24.6 ft below the bottom perforations adjacent to the target formation. Fig. 1 shows the completion diagram. The borehole azimuth at the tool depth is 94.2°N and the borehole deviation is 43° from vertical.

Two sets of continuous recordings were made during the injection and falloff phases. The first set of recordings was from 15:39 to 00:07 hours during a multirate injection and subsequent falloff. The second set ran from 09:21 to 12:00 hours during injection and a flowback test and a second injection and falloff (**Fig. 2**).

Data Processing and Analysis

Analog record sections containing apparent fracture signals were selected for digitization. These data also were recorded on audio tape. Three sets of 3,116 traces (one per component) of 186-msec-trace length were digitized at a sample rate of 0.04535 msec (4,100 samples per trace). This sample rate has a Nyquist frequency of 11,025 cycles/sec.

The frequency content of the data generally exceeds 1,000 cycles/sec, often reaching 1,500 cycles/sec. The traces were bandpass filtered from 150 to 2,000 cycles/sec with a sixth-order Butterworth filter and subsequently resampled at 0.0907 msec with a Nyquist frequency of 5,512 cycles/sec. A total of 215 events, thought to result from fracturing, were selected for further evaluation.

The fracture signatures are seen on all three components. Occasionally, the y axis shows low-frequency pump noise in the frequency range up to 300 cycles/sec, but frequency spectra of all three components during individual acoustic-emission events show similar trends. A broad trough in the y component around 700 cycles/sec is seen for several events, but, without high-frequency calibration, we cannot know whether this is related to the acoustic energy or the tool response. In any event, this should not affect the event locations because the first motions generally range at or above 1,000 cycles/sec. **Figs. 3 and 4** show sets of typical fracture signatures.

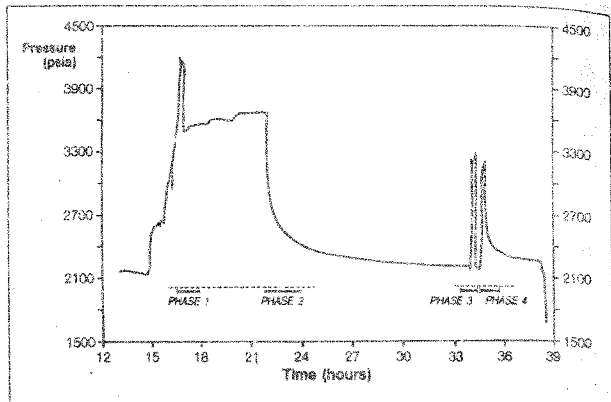

Fig. 2—Pressure curve. Recordings were made in time intervals indicated by dashed lines. First recording interval covers the multirate injection and falloff. Second interval contains injection with flowback, then injection with falloff. Events used for further processing were selected from time intervals shown by solid lines.

Arrival angles were determined by computing 2D crossplots of all pairs of components (hodograms) around the first cycle of the P-wave arrival for each event. Overall, the arrivals are oriented in the x-z plane.

To obtain an estimate of the hypocentral distance for a given event, we must identify a P- and an S-wave arrival. This is a nontrivial task and, in theory, should be done by crossplotting traces of particle displacement rather than acceleration. Liu and Helmberger[12] showed that, in cases of high-frequency seismic events, analysis of displacement and velocity waveforms is more reliable than that of acceleration waveforms. Accelerations can have polarizations and polarities that differ from the corresponding velocity and displacement waveforms.

If the P wave distributes its amplitude among the three tool components, the axes may need to be rotated into a coordinate system where one axis is along the P-wave arrival direction to identify the S-wave arrival. These arrival times can often be estimated or confirmed on the data traces.

The data recorded were particle accelerations, and, in many cases, it was sufficient to crossplot the particle accelerations, filtered as described earlier, to identify P- and S-wave arrivals. Some traces, however, had such high-frequency content that it was impossible to follow the trend of the hodograms, and it was necessary to integrate the traces to obtain particle velocity before proceeding with the hodogram analysis. Fig. 4 shows an example. Several schemes were tested, including filtering or further integration, to achieve displacement. The clearest hodograms were obtained with particle velocities.

Arrival times for P and S waves were identified for 18 events. The distance to an event is given by

$$L=(t_s-t_c)/[(1/v_s-1/v_c)], \quad \text{(1)}$$

where t_s and t_c are the S- and P-wave arrival times, and v_s and v_c are S- and P-wave velocities.

In the absence of sonic log data or seismic velocities from check shots or VSP's in this well, the velocities for the target formation were calculated with the following relationships for shaly sands,[13] given porosity and clay volume. Velocity values are in ft/s.

$$v_c=3.2808399(5.81-9.42\phi-2.21V_{cl}) \quad \text{(2)}$$

and $$v_s=3.2808399(3.89-7.07\phi-2.04V_{cl}), \quad \text{(3)}$$

or alternatively,[14]

$$v_c=3.2808399(5.59-6.93\phi-2.18V_{cl}) \quad \text{(4)}$$

and $$v_s=3.2808399(3.52-4.91\phi-1.89V_{cl}). \quad \text{(5)}$$

Average values for the target formation are $\phi=0.25$ and $V_{cl}=0.30$, giving ranges of 9,160 to 10,509 ft/s for v_c, and 4,954 to 5,659 ft/s for v_s. These correspond to slownesses of 109 to 95 μsec/ft for P waves and 201 to 176 μsec/ft for S waves. We used the average values of 9,836 ft/s for P waves and 5,308 ft/s for S waves to locate events. Although these formulas were developed on limited field and laboratory data, and different relationships may hold in the formation under consideration because of differences in mineralogy and grain structure, they serve as guides in the absence of real velocity data. For another well in Holland, check-shot P-wave velocities for this depth interval are about 15% higher than the P-wave velocity we used. This may indicate that our velocities are underestimated, but, because we cannot confirm the homogeneity of the formation over that distance, we cannot be sure a higher velocity is warranted. Uncertainty in the distance estimate, resulting from the empirical formula chosen and from observed ranges in the target formation ϕ and V_{cl}, is about ±6%, which does not include the uncertainty in the validity of the formulas. An additional error may be introduced by assuming a homogeneous formation with straight-ray propagation of seismic waves, but, in the present case, we do not have enough information to complicate our velocity model reliably.

Interpretation

Distribution of Events. A total of 215 events were selected for analysis. Although more events were identifiable, these were excluded because their relatively low amplitudes entailed poor signal-to-noise ratios (SNR's). Events were monitored throughout the four phases of the survey during the critical time intervals of injection and falloff. The majority of events were detected in Phase 3, the flowback test. The highest amplitude events occurred during falloff and flowback; periods of pressure increase were characterized by low-amplitude events.

Throughout the survey, the y axis was most sensitive to low-frequency borehole noise, either from the pump or fluid flow. Although few events exhibited first-arrival polarization with any significant component along the y axis, many events showed S-wave arrivals with large y amplitudes, confirming that the y axis was operational.

The first-arrival polarizations lie in the x-z plane that intersects the deviated well at the tool depth. A fan plot displays the arrival angles for events recorded in all four stages of the experiment (**Fig. 5**). The majority of events appear to originate in an area around the borehole and show no orthogonal S-wave arrival. Similar observations of borehole-oriented events were made in other acoustic-emission experiments monitoring minifractures in deviated wells[15] and were interpreted as refractions along the casing. At the relatively low frequencies contained in the data (100 to 1,200 cycles/sec), it is unlikely that a P wave would refract along the borehole and casing as a P or S wave, but it is possible, if the casing/cement bond were poor, that borehole-extensional modes could be excited in this frequency range. These modes would arrive at the tool with a first motion along the borehole axis and would not have an orthogonal S-wave arrival. In the case of hydraulic fracturing, it is possible that the cement will fracture along with the formation, but it is not clear why such arrivals should be prevalent simply because the well is deviated. By evaluating cement-bond quality before and after fracturing, it may be possible to determine whether the near-wellbore events result from cement fracturing.

A 180° ambiguity exists because the polarity of the first motion is not known. Most likely, however, the fracture noise occurs near the perforation interval above the tool. During the later phases of the fracture, particularly in the first reopening and subsequent flowback, several events originate from a direction perpendicular to the borehole.

Eighteen events contained S-wave arrivals that could be identified by particle acceleration (or velocity) rotated 90° with respect to P-wave arrival. The most distant event was approximately 148 ft from the sensor at an angle of 23° relative to the borehole, and all events arriving perpendicular to the borehole axis were located within 49 ft. Thus, all events lie within 66 ft of the borehole. The plane containing the events strikes N100°E east-southeast and dips 76° to the northeast, so the fracture plane is about 14° from vertical. **Fig. 6** shows the projection of the event locations on a vertical plane

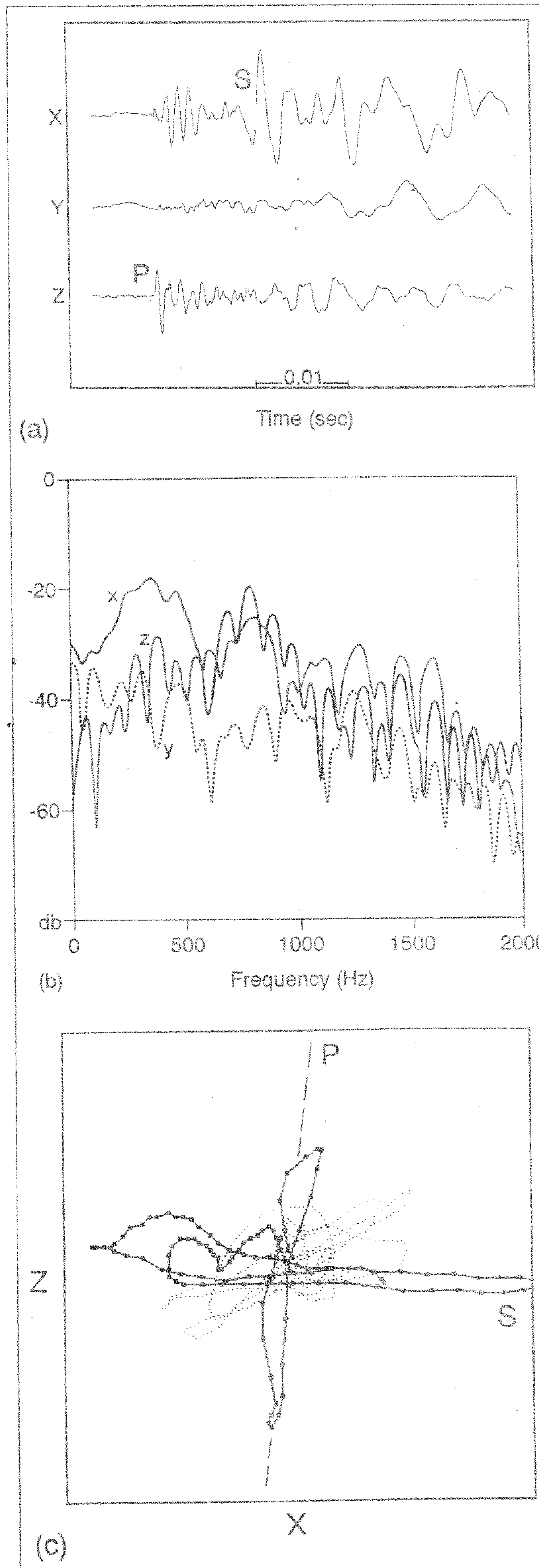

Fig. 3—(a) Fracture signal (acceleration) exhibiting P- and S-wave arrivals, (b) spectra for three components, and (c) particle motion crossplot (hodogram) for x and z axes.

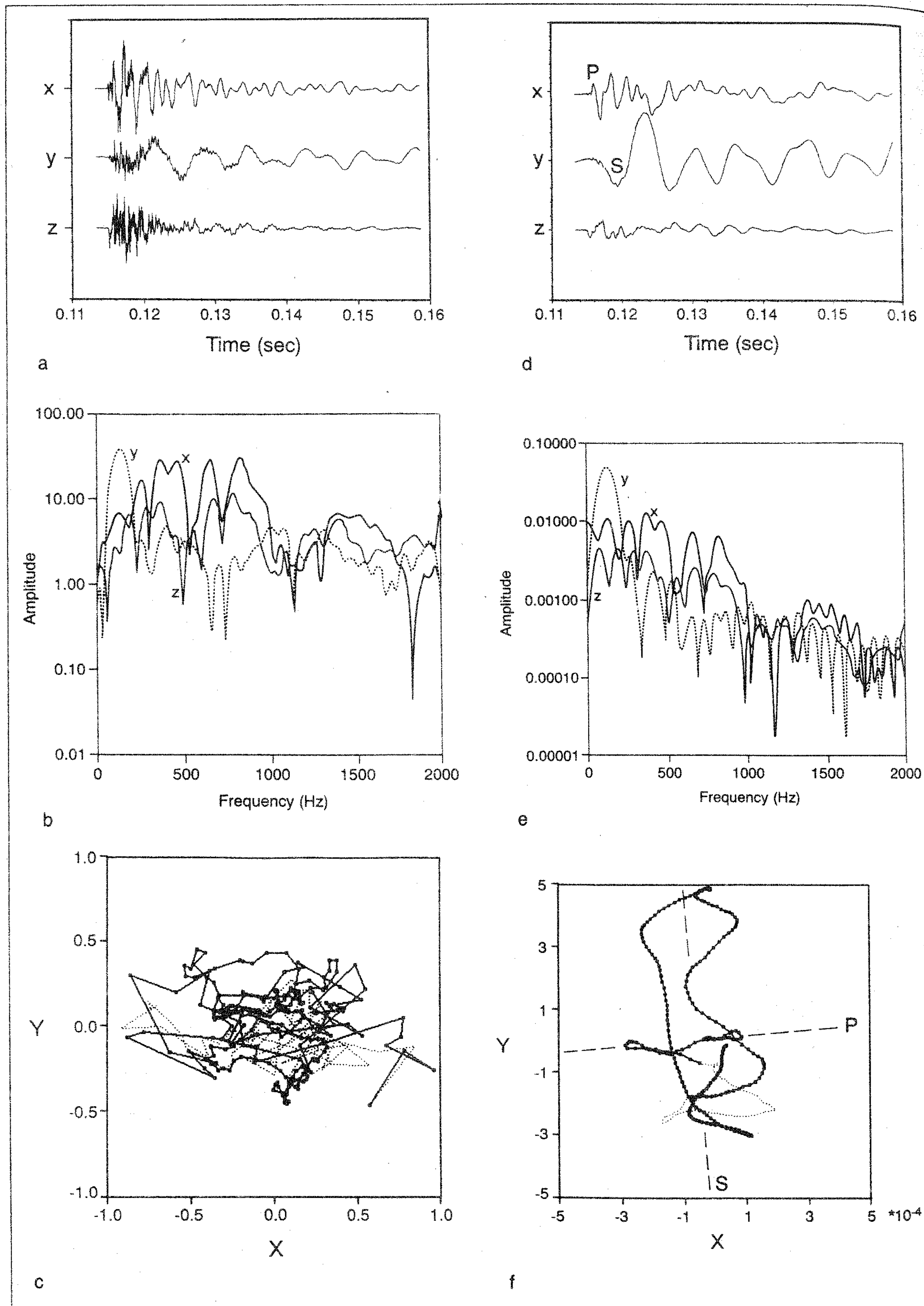

Fig. 4—(a) Fracture signal (acceleration), (b) spectra (acceleration signals), (c) *x-y* hodogram for acceleration signals, (d) integrated fracture signal (velocity), (e) spectra (velocity signals), and (f) *x-y* hodogram for velocity signal containing P- and S-wave motions.

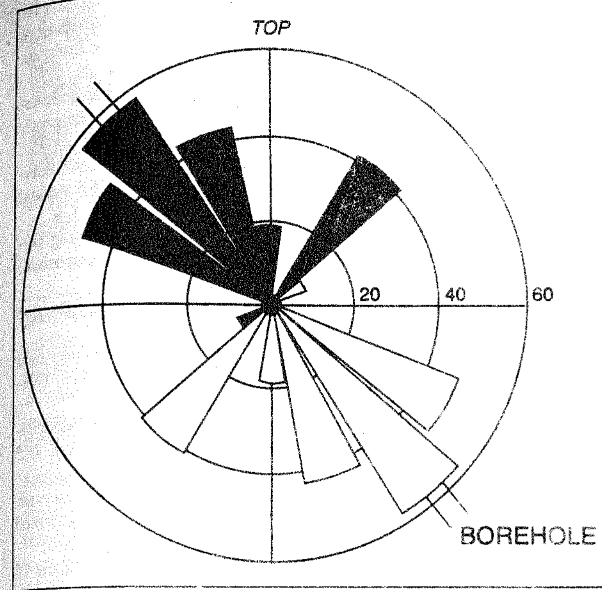

Fig. 5—Fan plot showing dominant arrivals in *x-z* plane for all events. Black regions indicate probable arrival directions.

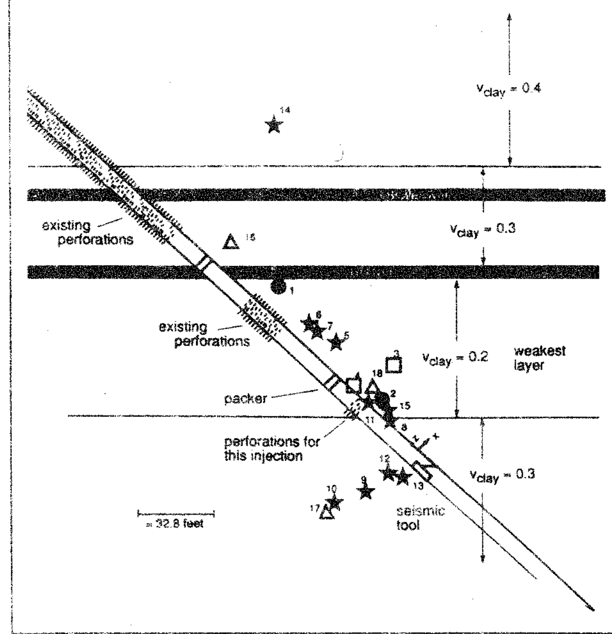

Fig. 6—Projection of event locations onto a vertical plane striking N100°E determined from 18 events containing identifiable P- and S-wave arrivals. Events in Fig. 2 are Phase 1 (●), Phase 2 (□), Phase 3 (★), and Phase 4 (△). Location numbers increase with time. Approximate V_{cl} were derived from a volumetric analysis of log information.

striking N100°E. Different symbols are used for the different phases of the experiment.

The azimuth of the fracture is within the range expected from stress measurements in the region. Borehole elongation, breakout, and televiewer data from wells in this area indicate that the regional maximum horizontal stress lies within the range north-northwest/south-southeast to west-northwest/east-southeast.[16,17] Hydraulic fractures in this stress field would have strikes in that range.

Correlation With Pressure Data. An analysis of the pressure measurements during the first shut-in can give a corroborating estimate of the fracture dimensions. The maximum fracture height is assumed to be 164 ft, as indicated by the vertical extent of the seismic activity, and its permeability is taken to be infinite. The Horner plot of pressure vs. time shows a change from linear to radial flow at very early time, indicating that the fracture has very little effect on the fluid flow in the formation. Curve-fitting yields a negative but very small skin effect, indicating that some wellbore stimulation has occurred. This could mean a small fracture or one of limited permeability. The best fitting model is for a fracture about 15 ft long. This agrees roughly with the acoustic-emission evidence in Fig. 6, indicating that the propagation of the fracture was limited horizontally; the area mapped out by the acoustic emissions is approximately 66 ft west-northwest/east-southeast by 164 ft in height. The different fracture length obtained by analysis of the pressure data corresponds to a length that remains open over the duration of the pressure measurement, while the length obtained from the seismic activity corresponds to any area that was once fractured and that subsequently closed.

Conclusions

Hydraulic fractures can be mapped by analyzing the accompanying seismic-energy release. We demonstrate the feasibility of the technique in the case of high-rate water injection in a sand/shale formation. Given our objective of determining fracture-propagation direction, we were able to record a large number of acoustic events during the critical stages of fracture opening and closing. Although we selected 215 events for further processing, the records showed many more low-amplitude events that evidently were related to the fracturing. Some of these events, however, may be related to cement fracturing around the casing. We expected that the best recordings would be made after shut-in; however, the SNR was good throughout all phases: injection, shut-in with falloff, and flowback. Real-time monitoring of the accelerometer signals during the fracture showed seismic activity during fracture opening. These observations coincided with those of the pumping crew during the test.

The events recorded were in the bandwidth from 100 to ≈1,200 cycles/sec. Eighteen events contained S-wave arrivals, enabling us to determine hypocentral distance. Results showed that it was better to use particle velocity rather than acceleration to determine particle motion from crossplots of the three components.

The locations of the seismic events map out an inclined planar area near the borehole. The plane strikes N100°E, dips 74° to the north, and is within the range of orientations expected given the regional stress field. The areal extent of the seismically active portion of the fracture is 164 ft high by 66 ft long.

Although the mapped fracture is not large, with real-time capability, this could be an effective way to control fracture jobs. By quantifying the fracture extent as it opens or closes, it may be possible to modify stimulation treatments and EOR programs to avoid or minimize breakthrough into stress barriers, to stop fractures with undesirable orientations, or to correct unsuccessful treatments.

Nomenclature

L = distance, ft
t_c = P-wave arrival time, seconds
t_s = S-wave arrival time, seconds
v_c = P-wave velocity, ft/sec
v_s = S-wave velocity, ft/sec
V_{cl} = clay volume, fraction
x,y,z = Cartesian coordinates, ft
ϕ = porosity, fraction

Acknowledgments

We thank Nederlanse Aardolie Mij. B.V. for permission to perform this test in one of their wells and to publish the technical data. We also acknowledge Westfälische Berggewerkschaftskasse (now Deutsche Montan Technologie GmbH) for the surface recording equipment used during acquisition. We are grateful to Schlumberger-Doll Research scientists H.-L. Liu and S.K. Chang for discussions related to this paper and Fikri Kuchuk for analysis of the pressure data. Thanks to M. Op-het-Veld of Schlumberger for the

Authors

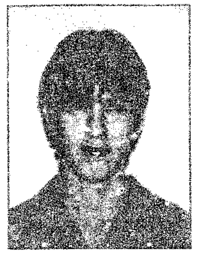

Stewart

Cassell

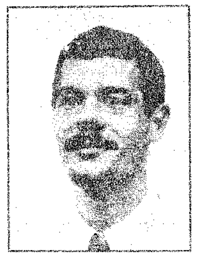

Bol

Lisa Stewart is a research scientist in the Interpretation Sciences Dept. at Schlumberger-Doll Research in Ridgefield, CT. She holds a BA degree from the U. of California, Berkeley, and MS and PhD degrees from Yale U., all in geophysics. She joined Schlumberger in 1985 to work on problems in geoacoustics and specializes in integrating seismic data with wireline data for reservoir characterization studies. **Bruce R. Cassell** is marketing manager for Schlumberger Wireline Services in Hannover, Germany. He holds a diploma in geophysics form the U. of Karlsruhe, West Germany, and a PhD degree in geophysics from Cambridge U. He joined Schlumberger in 1985 and has been a unit geophysicist in London and a division geophysicist in The Hague. His interests include borehole-seismic-processing techniques and their use to image subsurface structure, as well as the application of microseismic methods to delineate fine structure near the borehole. Cassell currently serves as secretary for the SPE German Section. **Gerard M. Bol** heads the drilling fluids and cement research group at Koninklijke/Shell E&P Laboratorium (KSEPL) in Rijswijk, The Netherlands. Gerard joined KSEPL in 1981, after graduating with an MS degree in chemical engineering from Delft Technical U., The Netherlands. For 6 years, he researched in drilling fluids, cement, and fracturing fluids, and in 1987, he went to work for Nederlanse Aardolie Mij. B.V. as a production technologist and appraisal engineer. He rejoined KSEPL in 1991.

hardware modifications of the downhole tool and to an anonymous reviewer whose suggestions were incorporated into this version of the paper.

References

1. *Reservoir Stimulation*, M.J. Economides and K.G. Nolte (eds.), Schlumberger Education Services, Houston (1987).
2. Pearson, C.: "The Relationship Between Microseismicity and High Pore Pressure During Hydraulic Stimulation Experiments in Low Permeability Granite Rocks," *J. Geophys. Res.* (1981) **86**, 7855-64.
3. Albright, J.N. and Pearson, C.F.: "Acoustic Emissions as a Tool for Hydraulic Fracture Location: Experience at the Fenton Hill Hot Dry Rock Site," *SPEJ* (Aug. 1982) 523-30.
4. Baria, R. and Green, A.: "Seismicity Induced During a Viscous Stimulation at the Camborne School of Mines Hot Dry Rock Geothermal Energy Project in Cornwall, England," *Proc.*, Progress in Acoustic Emission III, Japanese Soc. of NDI (1986) 407-29.
5. Niitsuma, H., Chubachi, N., and Takanohashi, M.: "Acoustic Emission Analysis of a Geothermal Reservoir and Its Application to Reservoir Control, *Geothermics* (1987) **16**, 47-60.
6. Dobecki, T.L.: "Hydraulic Fracture Orientation by Use of Passive Borehole Seismics," paper SPE 12110 presented at the 1983 SPE Annual Technical Conference and Exhibition, San Francisco, Oct. 5-8.
7. Wittrisch, C. and Sarda, J.P.: "SIMFRAC Method for Mapping Hydraulic Fractures," *Trans.*, 28th SPWLA Annual Logging Symposium, London (June 29-July 2, 1987) paper RR.
8. Thorne, B.J. and Morris, H.E.: "Advances in Borehole Seismic Fracture Diagnostics," *SPEFE* (Dec. 1988) 711-15.
9. Fix, J.E. *et al.*: "Developments of Microseismic Methods To Determine Hydraulic Fracture Dimensions," Technical Report No. 89-0116, Teledyne Geotech, Garland, TX (1989).
10. Deflandre, J.-P.: "Laboratory Analysis of Acoustic Emissions Associated With the Hydraulic Fracturing of Sandstone Samples," *Ref. IFP* (1989) 44, 673-91.
11. Green, A. and Baria, R.: "Active Seismics To Determine Reservoir Characteristics of a Hot Dry Rock Geothermal System," paper presented at the 12th Annual Geothermal Workshop, Stanford, Jan. 1987.
12. Liu, H.-L. and Helmberger, D.V.: "The 23:19 Aftershock of the 15 October 1979 Imperial Valley Earthquake: More Evidence for an Asperity," *Bull.*, Seis. Soc. Am. (1983) **75**, 689-708.
13. Castagna, J.P., Batzle, M.L., and Eastwood, R.L: "Relationships Between Compressional-Wave and Shear-Wave Velocities in Clastic Silicate Rocks," *Geophysics* (1985) **50**, 571-81.
14. Han, D.-h., Nur, A., and Morgan, F.D.: "Velocity Measurement and Empirical Modeling in Sandstones," *Trans.*, 27th SPWLA Annual Logging Symposium, Houston (June 9-13, 1986) paper OO.
15. Sarda, J.-P., Perreau, P.J., and Deflandre, J.-P.: "Acoustic Emission Interpretation for Estimating Hydraulic Fracture Extent," paper SPE 17723 presented at the 1988 SPE Gas Technology Symposium, Dallas, June 13-15.
16. Cox, J.W.: "Long Axis Orientation in Elongated Boreholes and Its Correlation With Rock Stress Data," *Trans.*, 24th SPWLA Annual Logging Symposium, Calgary (June 27-30, 1983), paper J.
17. Plumb, R.A. and Luthi, S.M.: "Analysis of Borehole Images and Their Application to Geologic Modeling of an Eolian Reservoir," *SPEFE* (Dec. 1989) 505-14.

SI Metric Conversion Factors

cycles/sec	× 1.0*	E+00	= Hz
ft	× 3.048*	E−01	= m
°F	(°F−32)/1.8		= °C
in.	× 2.54*	E+00	= cm
psi	× 6.894 757	E+00	= kPa

*Conversion factor is exact.

SPEFE

Original SPE manuscript received for review Oct. 22, 1990. Revised manuscript received Nov. 18, 1991. Paper accepted for publication Jan. 17, 1992. Paper (SPE 20970) first presented at the 1990 SPE European Petroleum Conference held in The Hague, Oct. 22-24.

Theory and Implementation of a Borehole Caliper Measurement Made While Drilling

W.C. Paske, SPE, **M.V. Rao**, SPE, **J.R. Twist***, SPE, **S.G. Mack**, and **R.L. Spross**, Sperry-Sun Drilling Services

Summary. Like comparable wireline measurements, measurement-while-drilling (MWD) formation-evaluation tools are dependent on the borehole condition. Because of this dependency, the borehole size must be known for appropriate borehole corrections to be made to porosity measurements. This paper describes caliper measurements that can compute the effective diameter of a uniform or nonuniform borehole with nonmechanical means. The basis for the caliper measurement is a gamma/gamma density sensor that uses asymmetric detector placement to define the borehole size. The derivation of the caliper is presented with field log comparisons.

Introduction

Because sensor capabilities are being added regularly to MWD systems, bottomhole-assembly (BHA) design must now contend with variables absent in the pre-MWD era. New considerations include MWD assemblies of a given OD that are less stiff than the BHA components they replace[1] and, depending on the particular drilling application desired, a different MWD sensor placed near the bit. Proximity of a given sensor to the bit is compromised further by the increasing use of steerable systems. These, by their very nature, require a motor near the bit, and directional sensors require additional nonmagnetic collars in proximity. All this requires that formation-evaluation-while-drilling (FEWD) sensors be placed as far as 200 ft from the bit. In some drilling environments, this can result in the borehole being significantly enlarged by the time FEWD sensors evaluate the rock.

Borehole enlargement is of particular concern for two reasons. First, from a drilling viewpoint, whether the hole enlargement occurs rapidly or slowly must be determined; i.e., is the borehole stable or unstable, and does knowing the stability of the borehole improve our understanding of the drilling conditions? Second, from a FEWD viewpoint, can we infer or measure the true borehole size so that the formation-evaluation sensors can be interpreted properly. This is very important in the case of nuclear formation-evaluation tools because, like standard wireline nuclear tools, they are very sensitive to borehole conditions. This borehole sensitivity implies that, to achieve formation-evaluation quality comparable with wireline, comparable knowledge of the borehole while drilling is necessary.

Borehole enlargement now can be measured while drilling with a nonmechanical sensor that uses multiple detector measurements to determine the average borehole caliber. This average can then be displayed as a continuous curve in the same manner as traditional mechanical calipers.

We calibrated the new borehole caliper measurements for various mud densities and borehole diameters. We observed that repeat sections or wiped logs after drilling indicate the same size or larger borehole. We obtained good agreement (within 3% to 10%) between dipmeter (x-y) caliper measurements and the measurements made while drilling and found that the geometric average of the wireline x-y dipmeter caliper was larger than or equal to the measurement made while drilling. These results were obtained at drilling rates of penetration (ROP's) of up to 500 ft/hr.

A borehole-size measurement made while drilling allows us to make the borehole corrections required by nuclear porosity sensors and to calculate the cement volume without making a separate trip into the borehole.

Design Constraints

MWD assemblies are used in the full range of well types, from straight-hole exploratory wells to horizontal wells. Consequently, these assemblies must be incorporated into the full gamut of BHA types. Nonmotor BHA designs are categorized as building, holding, and dropping assemblies.[2-4] The relative placement of only three full-gauge stabilizers near the bit produces the full range of desired angle changes, from aggressive build to aggressive drop. Small extents of undergauge on the blades (<0.5 in.) moderate aggressive assemblies. The foregoing emphasizes that the placement and diameter of stabilizers are key to controlling build/drop tendencies. To remain minimally intrusive to this process, we specified that our porosity sensor (and associated caliper device) design not require wall contact. This specification has the virtue of not complicating drilling situations where slick or near-slick assemblies are dictated by hole conditions. A final advantage is in pendulum dropping assemblies, where the closest available stabilizer is commonly 60 ft from the bit.

In addition, because the borehole is rarely circular, the caliper must be capable of making valid measurements in oval or elliptical boreholes. Finally, because the nuclear FEWD sensors are sensitive to the borehole size and environment (such as mud density), an MWD caliper must have an accuracy on the order of 0.125 in.

We imposed three restrictions, which are inherent to our MWD borehole caliper measurement: (1) there can be no mechanical protuberances to interfere with the drilling operation, (2) the caliper measurement must be capable of accurately averaging a noncircular borehole, and (3) the caliper must be accurate to 0.125 in.

Theory of Operation

To meet these restrictions, we used the Simultaneous Formation Density (SFD^{SM}) sensor to make the required measurements. The SFD sensor is the same gamma/gamma density tool described by Paske *et al.*[5] **Fig. 1** shows the tool in cross section. The basic tool has four detector banks on the circumference of an insert placed inside a drill collar. The detectors are placed with two axial spacings to the cesium-137 gamma source. The front detector bank in Fig. 1 is directly above the cesium source, and axially, is farthest from the source. The other three detector banks are placed at the same axial distance from the cesium source.

By placing the SFD tool in the various test pits shown in **Fig. 2**, the formation response of the individual detector banks can be determined as functions of the borehole diameter and the borehole mud density. These test pits consist of four limestone rock stacks and 12 density tanks. The tanks are used to determine the mud density effects on the nuclear sensors. **Fig. 3** shows the borehole dependence for one detector bank. The solid line fit in Fig. 3 is generated from the equations below.

$$I = I_0\alpha\,\exp[-m_0(\rho_b-\rho_m)] + I_0(1-\alpha)\exp[-\beta m_0(\rho_b-\rho_m)], \quad (1)$$

where $\beta=\exp[-k_1(d_h-d_t)/2]$ . . . . . (2)

and $\alpha=\exp[-k_2(d_h-d_t)/2]$. . . . . (3)

*Now at Develco Inc.